CCFE-PR(15)114

Yueqiang Liu, R. Akers, I.T. Chapman, Y. Gribov, G.Z. Hao,
G.T.A. Huijsmans, A. Kirk, A. Loarte, S.D. Pinches, M. Reinke,
D. Ryan, Y. Sun, Z.R. Wang

Modelling Toroidal Rotation Damping in ITER Due to External 3D Fields

Modelling Toroidal Rotation Damping in ITER Due to External 3D Fields

Yueqiang Liu[1,2,3], R. Akers[1], I.T. Chapman[1], Y. Gribov[4], G.Z. Hao[2], G.T.A. Huijsmans[4], A. Kirk[1], A. Loarte[4], S.D. Pinches[4], M. Reinke[5], D. Ryan[5], Y. Sun[6], Z.R. Wang[7]

[1] CCFE, Culham Science Centre, Abingdon, OX14 3DB, UK
[2] Southwestern Institute of Physics, PO Box 432, Chengdu 610041, China
[3] Department of Earth and Space Science, Chalmers University of Technology, SE-412 96 Gothenburg, Sweden
[4] ITER Organization, Route de Vinon-sur-Verdon, CS 90 046, 13067 St Paul-lez-Durance Cedex, France
[5] Department of Physics, University of York, Heslington, York, YO10 5DD, UK
[6] Institute of Plasma Physics, Chinese Academy of Sciences, PO Box 1126, Hefei 230031, China
[7] Princeton Plasma Physics Laboratory, Princeton University, PO Box 451, Princeton, NJ 08543-0451, USA

Modelling toroidal rotation damping in ITER due to external 3D fields

Yueqiang Liu[1,2,3], R. Akers[1], I.T. Chapman[1], Y. Gribov[4], G.Z. Hao[2], G.T.A. Huijsmans[4], A. Kirk[1], A. Loarte[4], S.D. Pinches[4], M. Reinke[5], D. Ryan[5], Y. Sun[6], Z.R. Wang[7]

[1] CCFE, Culham Science Centre, Abingdon, OX14 3DB, UK
[2] Southwestern Institute of Physics, PO Box 432, Chengdu 610041, China
[3] Department of Earth and Space Science, Chalmers University of Technology, SE-412 96 Gothenburg, Sweden
[4] ITER Organization, Route de Vinon-sur-Verdon, CS 90 046, 13067 St Paul-lez-Durance Cedex, France
[5] Department of Physics, University of York, Heslington, York, YO10 5DD, UK
[6] Institute of Plasma Physics, Chinese Academy of Sciences, PO Box 1126, Hefei 230031, China
[7] Princeton Plasma Physics Laboratory, Princeton University, PO Box 451, Princeton, NJ 08543-0451, USA

E-mail: yueqiang.liu@ccfe.ac.uk

Abstract. The linear and quasi-linear plasma response to the $n = 3$ and $n = 4$ (n is the toroidal mode number) resonant magnetic perturbation (RMP) fields, produced by the in-vessel edge localised mode control coils, is numerically studied for an ITER 15MA H-mode baseline Scenario. Both single fluid and fluid-kinetic hybrid models are used. The inclusion of drift kinetic effects does not strongly alter the plasma response compared to the fluid approximation for this ITER plasma. The full toroidal drift kinetic model is also used to compute the neoclassical toroidal viscous (NTV) torque, yielding results close to that of an analytic model based on geometric simplifications. The computed NTV torque from low-n RMP fields is generally smaller than the resonant electromagnetic torque for this ITER plasma. The linear response computations show a weak core kink response, contrary to a strong kink response often computed for plasmas from present day tokamak devices. Initial value quasi-linear simulations, including various torque models, show a localised damping of the plasma toroidal flow near the edge, as a result of the applied RMP fields. This localised rotation damping can be weak or strong depending on whether a weakly unstable edge localised peeling mode is present. No qualitative difference is found between the $n = 3$ and $n = 4$ RMP field configurations, in both the linear and non-linear response results.

1 Introduction

External three-dimensional (3D) magnetic field perturbations, such as intrinsic error fields or resonant magnetic perturbation (RMP) fields generated by magnetic coils, can have a profound influence on tokamak plasmas, which generally possess axi-symmetric (2D) equilibria. Whilst the low-n (n is the toroidal mode number) components of the error field are well known to produce, among other effects, mode locking phenomena in tokamaks [1], the RMP fields, often with tailored toroidal and poloidal spectra, are intentionally applied to mitigate or suppress the type-I edge localised modes (ELM) in ELMy H-mode plasmas [2, 3, 4, 5, 6, 7]. In ITER, three rows of in-vessel ELM control coils have been designed for this purpose.

Theoretical investigations of the effects, that external 3D fields have on tokamak plasmas, can be carried out at various levels of complexity. For instance, the vacuum model [8], single fluid model [9], 2-fluid models [15, 10, 11], and kinetic models [12, 13] have been adopted to study the RMP problem. Within the fluid model, both reduced magnetohydrodynamic (MHD) formulation [14, 15, 16] and full MHD [9, 10] have been considered. Following another classification, it is of interest to study the linear, quasi-linear, and non-linear plasma response to the external fields.

The linear response typically involves solving perturbed MHD equations, sometimes also in combination with linearised drift kinetic equations [12]. A steady state linear response solution, superposed on the 2D equilibrium, produces the so-called perturbed 3D equilibrium [17, 18]. This study has been shown to be very helpful in understanding several important aspects, including (i) the plasma induced 3D modification of the magnetic field structure, such as the field screening [19, 12], the field line ergodisation, the pitch resonant versus the kink-peeling plasma response [20]; (ii) the plasma displacement caused by the RMP fields as a results of the steady state plasma response [21, 22, 23]; (iii) the effect of the 3D plasma response field on energetic particle (EP) confinement.

The quasi-linear response study considers the self-consistent interaction between the $n \neq 0$ external field perturbation with the $n = 0$ plasma equilibrium quantities such as the toroidal flow. In this interaction, the plasma flow induced resonant field screening and the flow damping due to the 3D perturbation induced toques play key roles [24]. Therefore, the focus here is to investigate various possible torques acting on the plasma, due to the presence of 3D fields, such as the resonant electromagnetic torque, the torque associated with the neoclassical toroidal viscosity (NTV) [25, 26], and the Reynolds torque associated with the plasma inertia. In principle, there can also be torques associated with the 3D field induced redistribution of energetic particles (EPs), as well as the 3D field induced modification of intrinsic rotation. Since the various torques scale not only with the amplitude but also with the spectrum of the applied 3D field, it is important to investigate, for example, how the RMP field at different toroidal configurations (i.e. different n numbers) can affect the flow damping.

The non-linear study of the plasma response can be further classified into two categories: the (static) 3D equilibrium approach [27] and the (dynamic) initial value approach [29]. The full 3D equilibrium approach, contrary to the perturbed 3D equilibrium approach (from the linear response calculations), may provide a more accurate model of the plasma response (e.g. the 3D displacement) in particular near rational surfaces, although the final prediction may be sensitive to the plasma models that are used (ideal versus resistive plasma, static versus rotating plasma, etc.). The dynamic approach usually assumes resistive plasma, within either reduced or full MHD models, single or two-fluid approximations.

In this work, we focus our efforts on numerical modelling of both the linear and quasi-linear plasma response to the RMP field, for a 15MA ITER baseline scenario plasma [28]. We consider the ELM control coil currents both in the $n = 3$ and $n = 4$ configurations. Both a single fluid model and a MHD-kinetic hybrid model have been considered for the linear response study. The single fluid response model has previously been shown to successfully reproduce the experimental observations in the DIII-D RMP experiments, as long as the plasma pressure remains well below the Troyon beta limit [30]. The MHD-kinetic hybrid model is essential for predicting the plasma response in high beta plasmas [31]. We also use the drift kinetic model in the quasi-linear study, in order to provide more accurate computations of the NTV torque.

The computations are carried out using the MARS-F code [12] and the MARS-Q code [24], for the linear and the quasi-linear response, respectively.

Section 2 briefly introduces the toroidal response models. Section 3 describes the ITER equilibrium as well as the RMP coil configuration that we use in this study. Sections 4 and 5 report the computational results from the linear versus the quasi-linear models, respectively, followed by the concluding Section 6.

2 Toroidal plasma response models

The toroidal plasma response models that we use in this work have previously been introduced and tested. These include the single fluid RMP response model [9], the MHD-kinetic hybrid model [12], as well as the quasi-linear model [24]. Detailed discussions of the validity conditions for these models can be found in the above references. Below we briefly describe all these models, for the purpose of gathering all physics discussions associated with these models together, and more importantly, for facilitation of understanding the numerical results to be presented in later Sections.

The fluid model that we use for the RMP response consists of perturbed, single fluid, resistive MHD equations, with subsonic toroidal flow and flow shear, to be solved in the plasma region; the equation describing the RMP source term (the coil currents) to be solved in the vacuum region where the coils are located; equations for the perturbed magnetic fields in the vacuum region; and where applicable (e.g. with the ac RMP coil currents) the equation for the resistive wall(s), also located in vacuum. All these equations are self-consistently solved together.

The fluid equations for the plasma are written for the plasma displacement vector ξ, the perturbed velocity vector $\mathbf{v}$, the perturbed magnetic field $\mathbf{b}$, the perturbed plasma current $\mathbf{j}$, and the perturbed (fluid) pressure p

$$
\begin{aligned}
(\frac{\partial}{\partial t} + in\Omega)\xi &= \mathbf{v} + (\xi\cdot\nabla\Omega)R\hat{\phi}, && (1)\\
\rho(\frac{\partial}{\partial t} + in\Omega)\mathbf{v} &= -\nabla p + \mathbf{j}\times\mathbf{B} + \mathbf{J}\times\mathbf{b} - \rho\left[2\Omega\hat{\mathbf{Z}}\times\mathbf{v} + (\mathbf{v}\cdot\nabla\Omega)R\hat{\phi}\right] \\
&\quad -\rho\kappa_{\|}|k_{\|}v_{th,i}|\left[\mathbf{v} + (\xi\cdot\nabla)\mathbf{V}_0\right]_{\|}, && (2)\\
(\frac{\partial}{\partial t} + in\Omega)\mathbf{b} &= \nabla\times(\mathbf{v}\times\mathbf{B}) + (\mathbf{b}\cdot\nabla\Omega)R\hat{\phi} - \nabla\times(\eta\mathbf{j}), && (3)\\
\mathbf{j} &= \nabla\times\mathbf{b}, && (4)\\
(\frac{\partial}{\partial t} + in\Omega)p &= -\mathbf{v}\cdot\nabla P - \Gamma P\nabla\cdot\mathbf{v}, && (5)
\end{aligned}
$$

where R is the plasma major radius, $\hat{\phi}$ the unit vector along the geometric toroidal angle ϕ of the torus, $\hat{\mathbf{Z}}$ the unit vector in the vertical direction in the poloidal plane. The plasma resistivity is denoted by η. The equilibrium plasma density, field, current, and pressure are denoted by $\rho, \mathbf{B}, \mathbf{J}, P$, respectively. $\Gamma = 5/3$ is the ratio of specific heats. A conventional unit system is assumed with the vacuum permeability $\mu_0 = 1$. It is important to note that we solve for the full MHD equations. The solution variable $\mathbf{b}$ represents the *total* perturbed magnetic

field including the contributions from the plasma, the RMP coils as well as other conducting structures.

We assume that the (subsonic) plasma equilibrium flow $\mathbf{V}_0 = R\Omega\hat{\phi}$ has only the toroidal component, with Ω being the angular frequency of the toroidal rotation. A parallel sound wave damping term is added to the momentum equation (2), with κ being a numerical coefficient determining the damping "strength". $k_\parallel = (n - m/q)/R$ is the parallel wave number, with m being the poloidal harmonic number and q being the safety factor. $v_{th,i} = \sqrt{2T_i/M_i}$ is the thermal ion velocity, with T_i, M_i being the thermal ion temperature and mass, respectively. The parallel component of the perturbed velocity is taken along the equilibrium field line.

The RMP source term, i.e. the coil current $\mathbf{j}_{\rm RMP}$, is introduced via Ampere's law

$$\nabla \times \mathbf{b} = \mathbf{j}_{\rm RMP}. \tag{6}$$

Note that the above equation is solved in the vacuum region where the RMP coils are located.

In the presence of a resistive wall, the radial component of the field diffusion equation, or an equivalent form in the limit of the thin wall approximation, is solved

$$\frac{\partial b_r}{\partial t} = -[\nabla \times (\eta_w \nabla \times \mathbf{b})]_r, \tag{7}$$

where the subscript "r" denotes the radial component. η_w is the resistivity of the wall.

The vacuum equations, for regions not occupied by any conducting structures, are written for the (total) perturbed field

$$\nabla \times \mathbf{b} = 0, \qquad \nabla \cdot \mathbf{b} = 0. \tag{8}$$

Note that for the linear response model, if the source term $\mathbf{j}_{\rm RMP}$ is a dc current, or an ac current with given frequency $\omega_{\rm RMP}$, we are often interested in the steady state response, which can found by solving all the above equations, where the time derivative $\partial/\partial t$ is replaced by $i\omega_{\rm RMP}$ (with $\omega_{\rm RMP} = 0$ corresponding to the dc excitation).

In the MHD-kinetic hybrid model, we replace the fluid closure for the perturbed pressure, Eq. (5), by the following drift kinetic closure

$$\mathbf{p} = p_\parallel \hat{\mathbf{b}}\hat{\mathbf{b}} + p_\perp(\mathbf{I} - \hat{\mathbf{b}}\hat{\mathbf{b}}), \qquad p_\parallel = \sum_j \int M_j v_\parallel^2 f_j^1 dv, \quad p_\perp = \sum_j \int \frac{1}{2} M_j v_\perp^2 f_j^1 dv, \tag{9}$$

where the summation is carried out for all particle species. The perturbed distribution function f^1, which is the solution of the perturbed drift kinetic equation for each species, is normally divided into an "adiabatic" part f_a^1 and the "non-adiabatic" part f_L^1

$$f^1 = f_a^1 + f_L^1, \tag{10}$$

$$f_a^1 = \tilde{P}_\phi \frac{\partial f^0}{\partial P_\phi} - \mu \frac{|\mathbf{b}|}{B} \frac{\partial f^0}{\partial \mu}, \tag{11}$$

$$\frac{d f_L^1}{dt} = \frac{\partial f^0}{\partial \varepsilon} \frac{\partial H^1}{\partial t} - \frac{\partial f^0}{\partial P_\phi} \frac{\partial H^1}{\partial \phi} - \nu_{\rm eff} f_L^1, \tag{12}$$

$$H^1 = \frac{Ze}{c} \tilde{\mathbf{A}} \cdot \mathbf{v}_d - \mu |\mathbf{b}|, \tag{13}$$

where $f^0(P_\phi, \varepsilon, \mu)$ is the equilibrium distribution function of the particle, specified in terms of three constants of motion of the particle: the toroidal canonical momentum P_ϕ, the energy ε and the magnetic moment μ. $\tilde{P}_\phi$ denotes the perturbed P_ϕ. H^1 is the perturbed particle Lagrangian, with $\tilde{\mathbf{A}}$ being the perturbed magnetic vector potential and $\mathbf{v}_d$ being the drift velocity of the particle. ν_{eff} is the effective collision frequency (of the Krook collision operator). We have neglected the perturbed electrostatic potential in our drift kinetic model. The MARS-K drift kinetic module has been successfully benchmarked against the HAGIS code [12] and other hybrid codes based on the perturbative approach [32], for the stability computations of the resistive wall mode.

The quasi-linear response model solves the above linear response equations together with the $n = 0$ toroidal momentum balance equation for $L = \rho < R^2 > \Omega$, as an initial value problem,

$$\frac{\partial L}{\partial t} = D(L) + T_{\text{source}} + T_{\text{NTV}} + T_{j\times b} + T_{\text{REY}}. \tag{14}$$

The right hand side of Eq. (14) includes the momentum diffusion term $D(L)$, the momentum source term T_{source} representing, e.g. the momentum input from neutral bean injection, as well as various momentum sink terms, such as the the toroidal component of the NTV torque T_{NTV}, the resonant electromagnetic torque $T_{j\times b}$, and Reynolds torque T_{REY} associated with the inertial term $\rho(\mathbf{v}\cdot)\mathbf{v}$. Detailed description of each term can be found in Ref. [24]. In the model presented here, the NTV and $\mathbf{j}\times\mathbf{b}$ torques are due solely to the application of 3D RMP fields. Therefore, if we assume that, before the application of the RMP fields, an equilibrium torque balance has been reached, we can solve for an equation for the change of the momentum ΔL. In this equation, the momentum source term drops out.

We have two models to evaluate the NTV torque. One is based on the smoothly connected analytic formulas [25] which have been implemented into MARS-Q [24]. The drift kinetic formulation in MARS-K provides another tool to compute the NTV torque which, as has been shown [33, 34], is inherently related to the perturbed drift kinetic energy perturbation

$$T_{\text{NTV}} = -2n\text{Im}(\delta W_k), \tag{15}$$

where $\delta W_k = -1/2\int(-\nabla\cdot\mathbf{p})\cdot\xi_\perp^* d^3x$. Reference [34] also numerically benchmarked these two NTV models between MARS-Q and MARS-K, not only for the net torque amplitude but also for the flux surface averaged radial torque density.

We also mention the typical boundary conditions that we apply for solving the momentum balance equation. At the magnetic axis, the free (Neumann) boundary condition is assumed. At the plasma edge, we assume a homogeneous Dirichlet boundary condition for ΔL. For tokamak plasmas, this is a reasonable approximation of the more generic Robin boundary condition, as demonstrated in Ref. [1].

An adaptive time-stepping scheme is envisaged for solving the quasi-linear response problem. The MARS-Q modelling results have been successfully compared with the RMP experiments in MAST [35].

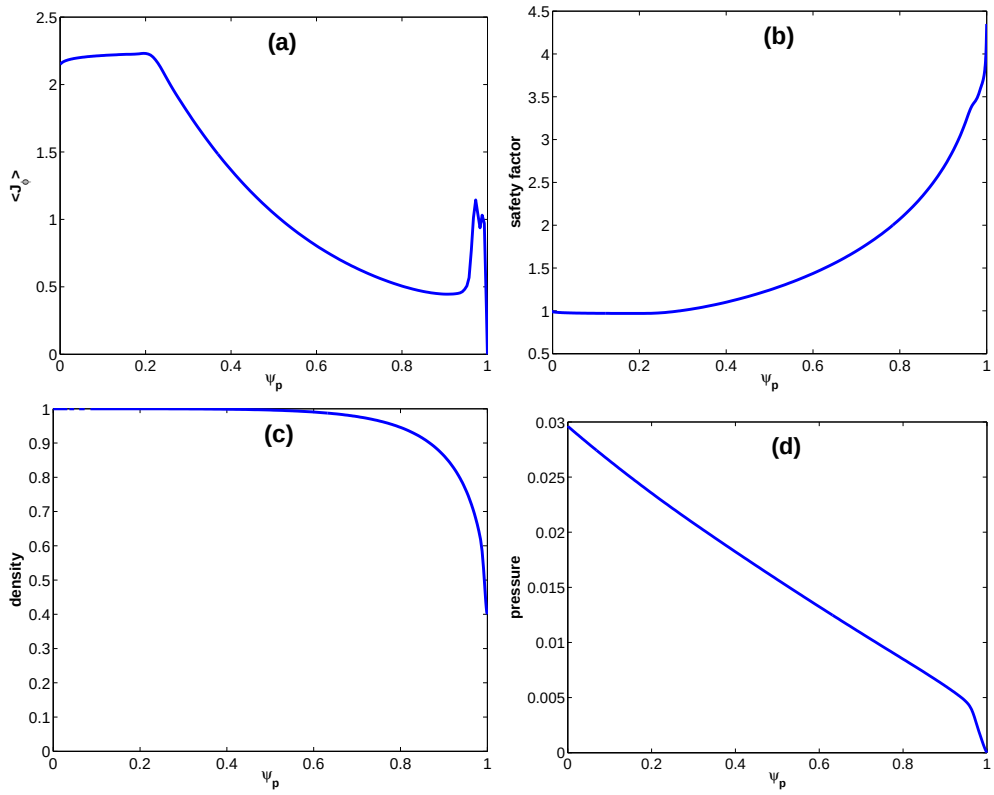

Figure 1: Equilibrium radial profiles for (a) the surface averaged toroidal plasma current density, (b) the safety factor q, (c) the plasma density, and (d) the plasma pressure, for the ITER baseline 15MA plasma at burning condition. The plasma minor radius is labelled by the normalised equilibrium poloidal flux ψ_p.

3 Equilibrium and coil configuration

We consider an ITER equilibrium from the 15MA, $Q_{DT} = 10$ baseline scenario under burning condition. Figure 1 shows the key equilibrium radial profiles, obtained from the CORSICA [36] self-consistent transport simulations. The plasma has a pedestal top temperature of 4.4keV. The surface averaged toroidal plasma current density $< J_\phi >$ is normalised by $J_0 \equiv B_0/(\mu_0 R_0)$, with $B_0 = 5.3$Tesla, $R_0 = 6.2$m, $\mu_0 = 4\pi \times 10^{-7}$H/m. The plasma number density is normalised to unity at the magnetic axis. The plasma pressure is normalised by $P_0 \equiv B_0^2/\mu_0$. This H-mode plasma has a pedestal top temperature of 4.4keV. The strong bootstrap current near the plasma edge (Fig. 1(a)), due to the pressure pedestal (Fig. 1(d)), has a clear effect on the q-profile near and beyond the q_{95} surface (Fig. 1(b)).

There are three sets of in-vessel ELM control coils according to the ITER design: the upper (U), middle (M) and lower (L) set, respectively. The modelled coil geometry is shown in Fig. 2(a). Each set consists of 9 coils along the toroidal angle. Note that the poloidal coverage of the upper, middle and lower sets of coils vary, as more clearly shown in the $R-Z$ plane in Fig. 2(b). The plasma boundary shape, as well as the modelled double wall shapes, is also shown in this figure. Note that we slightly smooth the plasma boundary near the X-point, since our computational model, based on the magnetic flux based coordinate system, cannot resolve the exact X-point geometry. This smoothing has very little effect on the q_{95} value which is

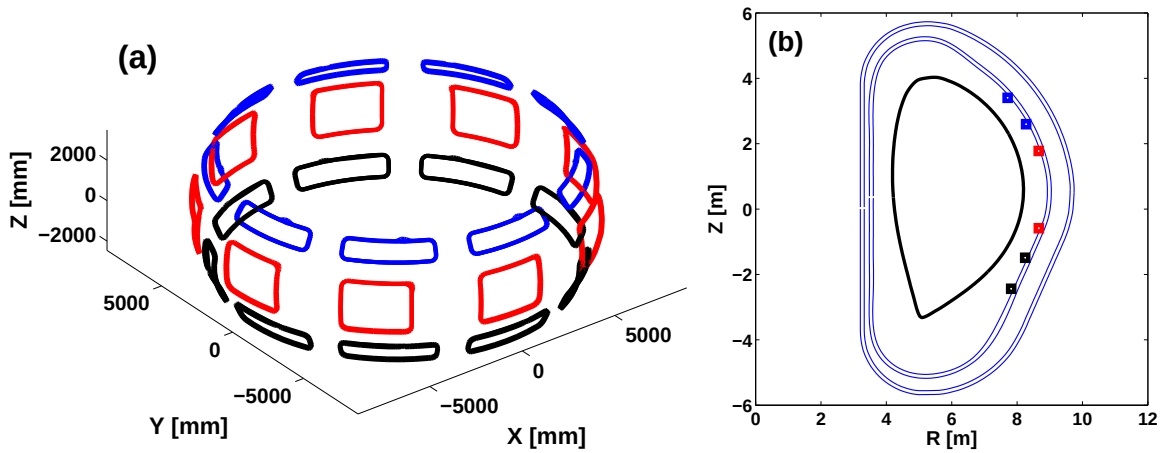

Figure 2: (a) Geometry of the modelled in-vessel ELM control coils in ITER. The location of these three sets of coils is also indicated in the poloidal plane shown in (b), together with the plasma boundary and the double vacuum vessel.

about 3.18, but does sensitively change the edge q value at the plasma surface. For the plasma surface shape shown here, the q_a value is 4.33 as shown in Fig. 1(b).

Outside the plasma surface, we have the vacuum region (no scrape-off-layer is modelled) and other conducting structures. In particular, the double wall conducting structures are modelled as complete walls in this work. This approximation is acceptable for low frequency RMP response computations. Here we assume that the applied RMP field rotates at 1Hz along the toroidal direction. With this nearly static field perturbation, the vacuum vessel, as well as other conducting structures surrounding the plasma, plays a minor role.

The coil currents are arranged to produce predominantly the $n = 3$ or the $n = 4$ toroidal Fourier components of the vacuum magnetic field. In the nominal modelling cases, we consider either the $n = 3$ coil current at 45kAt, or the $n = 4$ current at 30kAt. For the $n = 3$ configuration, the toroidal phases of the upper and lower coil currents, with respect to the middle one, are $\phi_U = \phi_M - 82.7^o$, and $\phi_L = \phi_M - 30.7^o$, respectively. For the $n = 4$ configuration, we set $\phi_U = \phi_M - 48.7^o$ and $\phi_L = \phi_M - 34.7^o$. These current phases are optimal according to the Chirikov parameter based vacuum field criteria [37].

4 Linear response

In the linear response computations, we are primarily interested in three aspects: the perturbed magnetic field with the inclusion of the plasma response and a comparison with the vacuum field; the RMP induced plasma boundary displacement for this ITER plasma; and the toroidal torques acting on the plasma due to the applied RMP field, in particular the NTV torque due to the presence of 3D magnetic field perturbations. All these aspects generally depend on the plasma model. Here we compare the computational results from a single-fluid resistive plasma response model and from a self-consistent MHD-drift kinetic hybrid model. These models are described in Section 2. The plasma resistivity follows the Spitzer model,

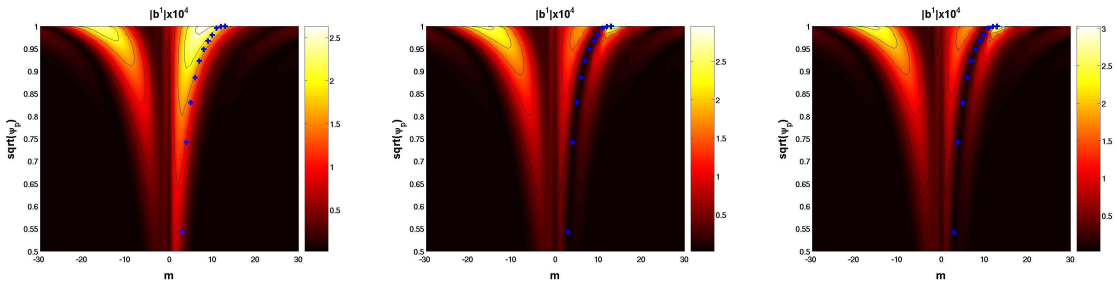

Figure 3: Poloidal spectrum of the perturbed radial field b^1 from (a) the vacuum approximation, (b) the resistive fluid plasma response, and (c) the resistive drift kinetic plasma response. The $n = 3$ RMP coil current configuration is assumed. The symbol '+' indicates the location of rational surfaces for the $n = 3$ perturbation.

which gives the on-axis Lundquist number of $S(0) = 8 \times 10^9$ for this ITER plasma, where $S = \tau_R/\tau_A, \tau_R = \mu_0 a^2/\eta, \tau_A = R_0\sqrt{\mu_0\rho_0}/B_0$, with η being the plasma resistivity and ρ_0 being the on-axis plasma density. The radial profile of S scales with the thermal electron temperature as $T_e^{3/2}$. Both the $n = 3$ and $n = 4$ coil configurations are investigated.

4.1 $n = 3$ RMP coil configuration

The poloidal spectra of the computed radial fields are compared in Fig. 3, for the vacuum approximation, the resistive fluid plasma response, and the drift kinetic plasma response, respectively. The self-consistent kinetic plasma response includes the precessional drift resonances of both thermal ions and electrons, as well as the bounce and transit resonances of thermal ions.

The perturbed radial field is defined as

$$b^1 = \frac{\mathbf{b} \cdot \nabla\psi}{\mathbf{B}_{\rm eq} \cdot \nabla\phi} \frac{q}{R_0^2 B_0}. \tag{16}$$

Note that this is a dimensionless quantity according to the above definition. The poloidal Fourier harmonics of b^1 are defined in the PEST-like straight field line coordinate system (with the jacobian being proportional to R^2). Shown in Fig. 3 is the amplitude of the poloidal harmonics inside the plasma, between $s \equiv \sqrt{\psi_p} = 0.5$ and 1. The field amplitude is small in the plasma core, compared to that near the edge. With the RMP coil geometry and the chosen toroidal phasing of the coil currents, the vacuum field is close to, but does not perfectly match, the maximal field pitch resonance. With the inclusion of the plasma response, the resonant field amplitude is significantly reduced almost everywhere inside the plasma except near the very edge (where the high $m > nq_a$ peeling mode harmonics is slightly amplified), as shown in Figs. 3(b) and (c). For this ITER plasma, both fluid and kinetic models produce similar plasma response (both spectra and amplitude). Unlike the typical plasma response computed for MAST [35] or DIII-D [20] where a significant core kink response induced field amplification often (but not aways) occurs, no such kink response is observed for this ITER case.

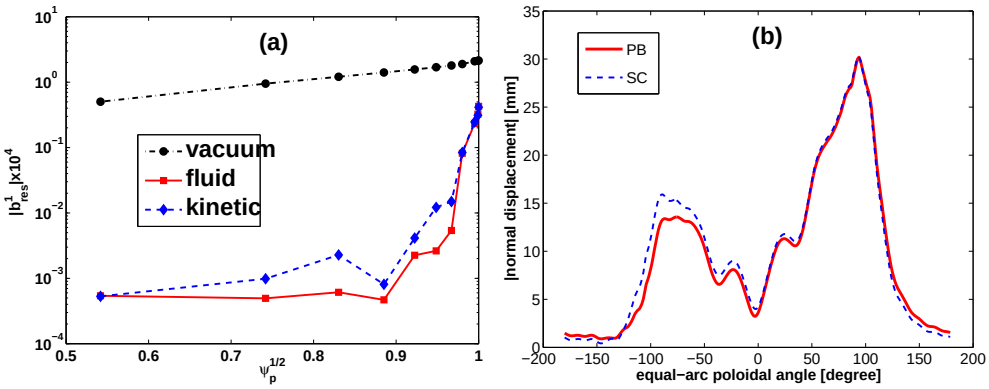

Figure 4: Comparison of (a) the resonant harmonic amplitude for the perturbed radial field b^1_m, and (b) the normal displacement of the plasma surface, between the resistive fluid plasma response (solid lines and labelled "PB") and the self-consistent drift kinetic plasma response (dashed lines and labelled "SC"). The vacuum field (dashed-dotted line) is also plotted in (a). The $n = 3$ coil current configuration is assumed.

The amplitude of the pitch resonant fields is further compared in Fig. 4(a). Again we observe a significant reduction of the field amplitude compared to the vacuum field. The fluid and the kinetic plasma models produce similar response not only in terms of the response field, but also in the plasma surface displacement as shown in Fig. 4(b). The similarity between the two types of response is probably due to the fact that the plasma pressure is relative low ($\beta_N = 1.86$) for this ITER plasma, so that the fluid approximation is still largely valid for describing the plasma response [30]. The predicted maximal plasma surface displacement is about 30mm with the 45kAt of the $n = 3$ RMP coil current. The fact that the displacement does not peak near the outboard mid-plane (at the poloidal angle $\simeq 0$), again reflects the lack of the kink response - a correlation (between the core kink response and the mid-plane displacement) as has been found in the modelling of the MAST plasmas [22].

Figure 5(a) compares the NTV torque density computed by two models - the MARS-Q model [24] and the MARS-K model [12]. The MARS-Q model is based on the smoothly connected analytic formulas obtained from analytic solution of the bounce averaged drift kinetic equation under geometric simplifications. The MARS-K model is based on the numerical solution of the drift kinetic equation with full toroidal geometry. These two models have been successfully benchmarked on a large aspect ratio plasma [34]. The agreement between these two models still largely holds even for a more complicated equilibrium as shown here, as long as the same physics are assumed in both models (i.e. the precessional drifts of thermal ions in this comparison). The net NTV torque mostly comes from the plasma edge region, where the MARS-K model predicts a somewhat higher torque density than the MARS-Q model.

The computed NTV torque is due mainly to the so-called non-resonant component in most of the plasma region. This can be understood from a comparison of various frequencies shown in Fig. 5(b). The effective collision of thermal ions is very low (compared to other drift frequencies) in the ITER plasma, as expected. The fact that the precessional drift frequency ω_D of thermal ions is small, compared to the $\mathbf{E} \times \mathbf{B}$ drift frequency ω_E in the bulk of the plasma, excludes the possibility of generating a large NTV torque associated with the resonance effect. Therefore, the NTV torque is largely from the non-resonant contribution in this ITER plasma.

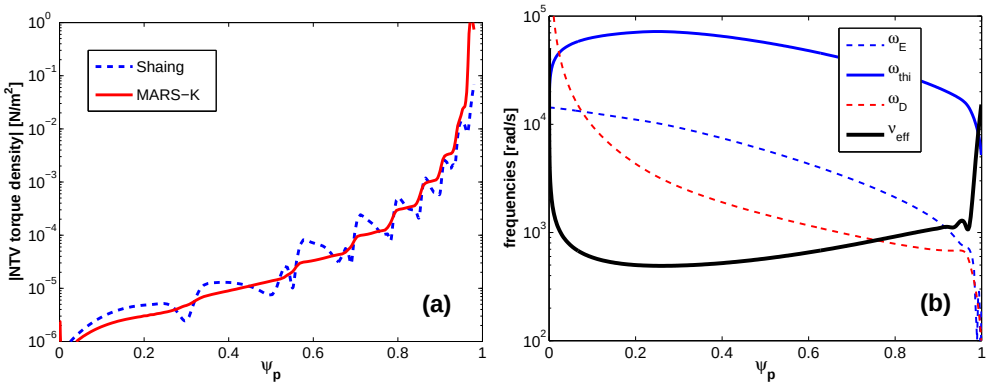

Figure 5: Comparison of (a) the NTV torque density due to the precessional drift resonance of thermal ions (Shaing's analytic theory solution versus full toroidal MARS-K solution), and (b) various frequencies (the $\mathbf{E}\times\mathbf{B}$ frequency ω_E, the thermal ion sound frequency ω_{thi}, the thermal ion precessional drift frequency ω_D at the particle thermal speed, as well as the thermal ion effective collision frequency $\nu_{\rm eff}$). The resistive fluid response is used for evaluating the NTV torque. The $n=3$ coil current configuration is assumed.

The above analysis does not apply to the very edge of the plasma, where even the condition of the bounce averaged drift kinetic approximation, assumed in the MARS-Q model, is not anymore satisfied. This approximation assumes that all the drift frequencies should not exceed the frequency $\omega_{\rm thi}$ associated with the particle thermal speed,

Due to the lack of the resonance induced enhancement, the NTV torque is relatively small in this ITER plasma. In fact the computed NTV torque, as well as the Reynolds stress torque, is typically one order of magnitude smaller than the resonant electromagnetic torque (the $\mathbf{j}\times\mathbf{b}$ torque) as will be shown in Section 5. This holds also for the $n=1$ RMP response that we have tested.

MARS-K also has the capability of computing the NTV torques generated by other drift motions of particles, such as the bounce (for trapped particles) and transit (for passing particles) motions. Figure 6 compares the torque density associated with various particle drifts, including as well the contribution from the toroidal precession of thermal electrons. Even though the bounce and transit drifts of thermal particles contribute a larger torque density in the plasma core region, than the thermal ion precessional drift, the net torque still largely comes from the precessional drifts of thermal ions and electrons near the plasma edge. The torque densities shown in Fig. 6 are computed by using the (same) plasma response solution from the fluid model. Using the same response function makes it easier to compare the various contributions of the NTV torque. This can be viewed as a perturbative approach.

4.2 $n=4$ RMP coil configuration

We also perform similar studies of the RMP response to the $n=4$ coil configuration, in terms of the perturbed field, the plasma surface displacement, and the NTV torques. The results are summarised in Figs. 7-9, respectively.

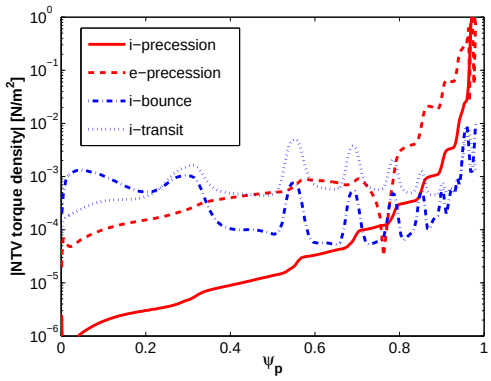

Figure 6: Comparison of the NTV torque density from various drift resonance contributions (precessional drift of thermal ions/electrons, bounce/transit drift of thermal ions). The fluid plasma response solution is used for evaluating the NTV torque. The $n = 3$ coil current configuration is assumed.

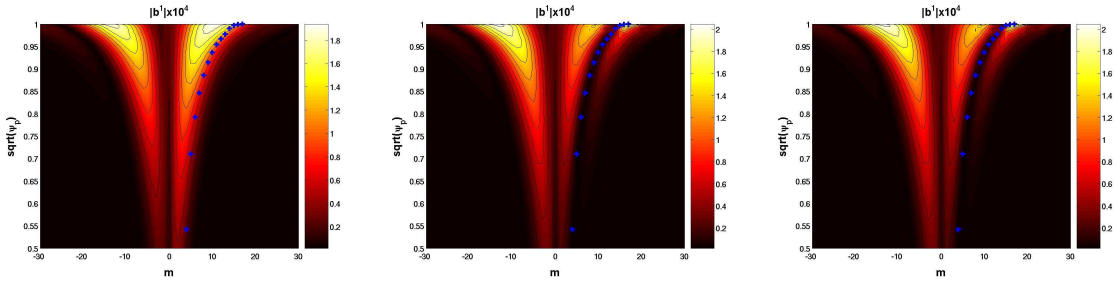

Figure 7: Poloidal spectrum of the perturbed radial field b^1 from (a) the vacuum approximation, (b) the resistive fluid plasma response, and (c) the resistive drift kinetic plasma response. The $n = 4$ RMP coil current configuration is assumed.

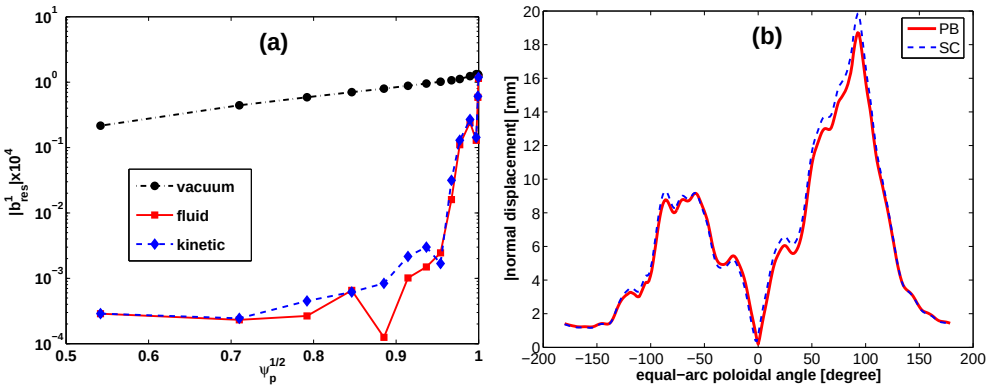

Figure 8: Comparison of (a) the resonant harmonic amplitude for the perturbed radial field b^1_m, and (b) the normal displacement of the plasma surface, between the resistive fluid plasma response (solid lines) and the self-consistent drift kinetic plasma response (dashed lines). The vacuum field (dashed-dotted line) is also plotted in (a). The $n = 4$ coil current configuration is assumed.

In general similar observations are made between the $n = 3$ and the $n = 4$ configurations, in all of the above aspects. The agreement between the fluid response and the drift kinetic response appears to be even better for the $n = 4$ configuration. The computed maximal plasma surface displacement is just below 20mm with the $n = 4$ configuration, probably due to the combined effects of smaller current amplitude (45kAt for $n = 3$ versus 30kAt for $n = 4$), and the radially faster decay of the $n = 4$ field.

5 Quasi-linear results

One free parameter in our quasi-linear model is the momentum diffusion coefficient, which is generally assumed to be a function of the plasma minor radius [24]. Various diffusion models have been included into the MARS-Q implementation, though generally no sensitive dependence of rotation damping on the momentum diffusion profile has been found [24, 35]. In this work, we choose the diffusion profile that scales with $T_e^{-3/2}$, with the core value of the diffusion coefficient of the order $\sim 1m^2/s$.

It is known that for a limiter configuration (which is what we effectively obtain after slightly smoothing the plasma boundary surface near the X-point for the original ITER plasma in the divertor configuration), the linear stability of the peeling mode is sensitive to the edge safety factor q_a. Computational examples are shown in Ref. [38]. The quasi-linear initial value solution of the RMP response is also sensitive to q_a, as will be shown later on. In order to demonstrate that it is the linear stability (as opposed to the non-linear interaction between the field penetration and the rotational damping) that largely dictates the evolution of the quasi-linear solution, we first run MARS-Q without the non-linear coupling effect. To achieve this, we (artificially) do not apply the momentum sink terms (various torques) to the $n = 0$ momentum balance equation, thus effectively fixing the flow speed at the initial, equilibrium value.

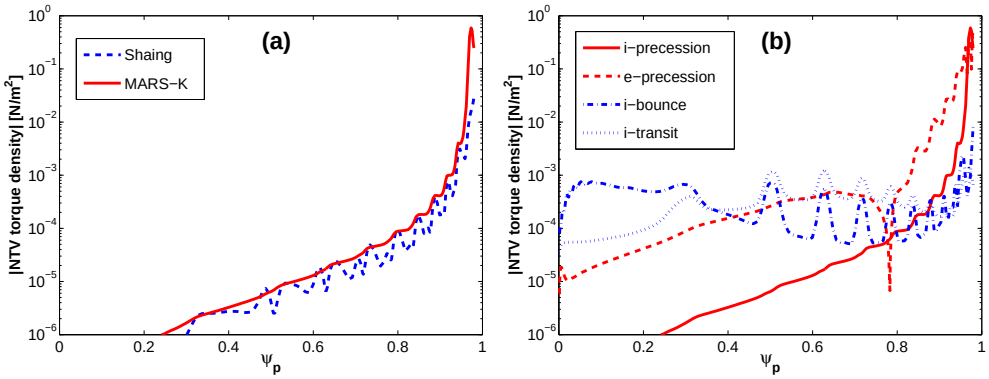

Figure 9: Comparison of the NTV torque density (a) due to the precessional drift resonance of thermal ions between Shaing's analytic theory solution and full toroidal MARS-K solution, and (b) due to various drift resonance contributions (precessional drift of thermal ions/electrons, bounce/transit drift of thermal ions) with the MARS-K model. The resistive fluid response is used in all cases. The $n = 4$ coil current configuration is assumed.

Figure 10 compares the results from four such runs with the $n = 3$ RMP configuration, with q_a values at 4.33,4.19,4.07,3.94, respectively. Note that the change of q_a is achieved by slightly smoothing the plasma boundary shape near the X-point. This leaves unchanged the bulk q-profile, as well as the other global equilibrium parameters such as the total plasma current. In particular, the q_{95} remains the same at 3.18. The boundary shape shown in Fig. 2(b) corresponds to $q_a = 4.33$. Figure 10 plots the time evolution of the computed net torques as an indicator to the stability of the linear response. With progressively more smoothing applied to the X-point, corresponding to the decrease of q_a, the response becomes more unstable, which manifests the transition from a linearly stable peeling mode (at $q_a = 4.33$) to a linearly unstable peeling mode (at $q_a = 3.94$). The stability boundary is near the integer number of $q_a = 4$ in our case. We point out that the existence of an exact X-point corresponds to an infinite q-edge value (with a logarithmic weak singularity). The associated stronger singularity of the magnetic shear near the separatrix tends to make the edge localised peeling mode marginally stable [39, 40]. In real experiments, an infinite q value is probably not expected. Nevertheless, this ideal case of a marginally stable peeling mode response, due to the X-point stabilisation, is mimicked here by studying the transition from a weakly unstable to a weakly stable peeling mode, by tuning the q_a value.

The case (a) (with $q_a = 4.33$) is clearly a stable solution. The linear response computations, shown in Section 4, are performed for this case. It is expected that the saturated initial value solution for this case should recover that found from the direct linear response computation in the frequency domain, as shown in Fig. 4. Indeed we checked both solutions, and found that they agree with each other.

We point out that the net torques shown in Fig. 10 mainly come from the contribution near the plasma edge. The core torque density is small. For a comparison of the order of magnitude, Fig. 6 shows the computed core NTV torque density of the order of 10^{-3}[N/m^2] (the highest values), compared to the order of 10^{-1}[N/m^2] negative neutral beam driven torque as predicted by the TRANSP simulation for ITER H-mode plasmas [41].

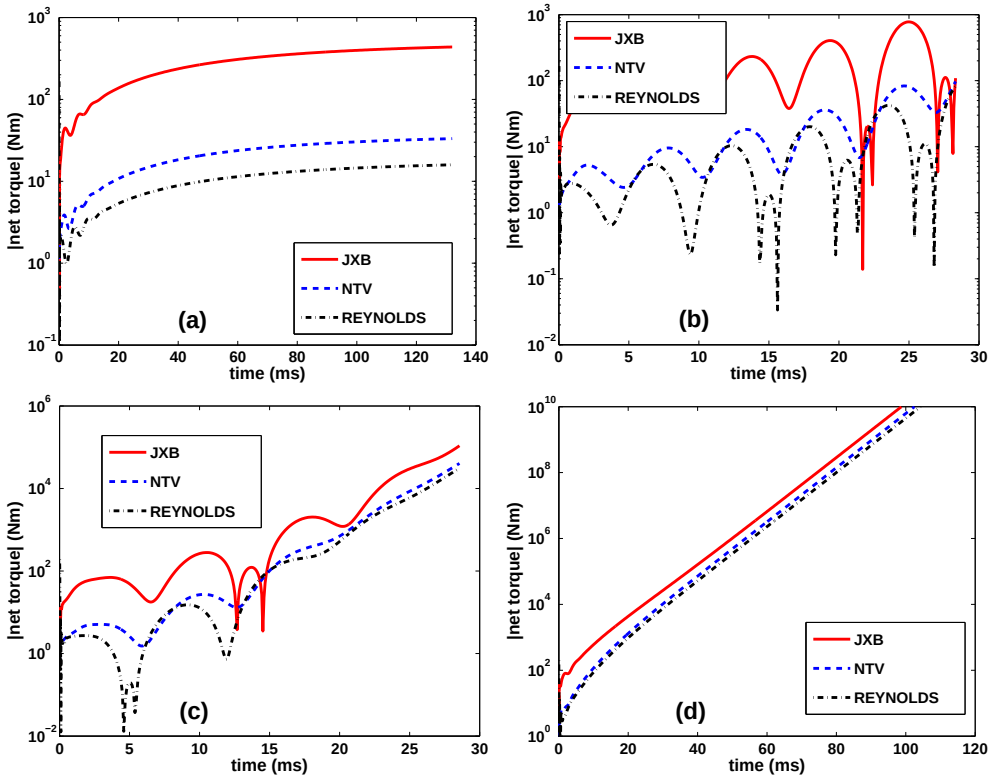

Figure 10: The amplitude of the computed net torques from the initial value simulations of the plasma response to the $n = 3$ RMP fields with fixed flow (i.e. in the absence of non-linear coupling to flow damping), for the same ITER plasma and coil configurations, but with slightly different assumption on the edge q-value: (a) q_a=4.33, (b) q_a=4.19, (c) q_a=4.07, (d) q_a=3.94.

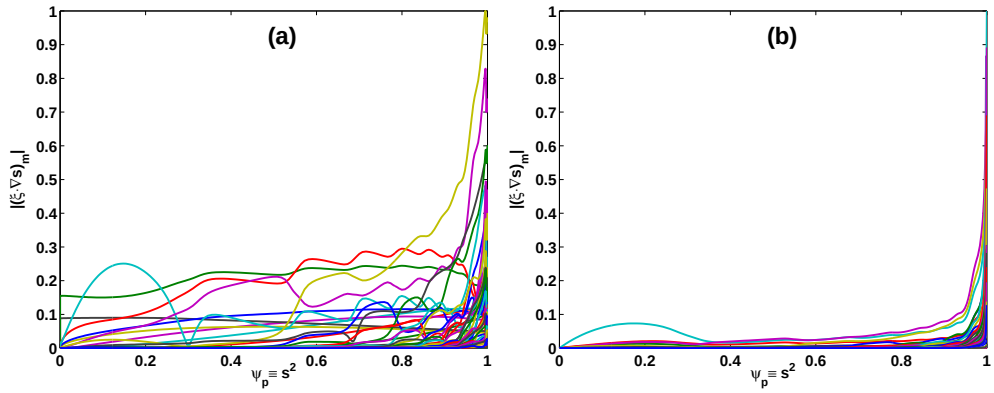

Figure 11: The normalised amplitude of the poloidal Fourier harmonics for the radial displacement, from the plasma response computations shown in Fig. 10, for the case of (a) q_a=4.33 and (b) q_a=3.94. The Fourier harmonics are decomposed in the equal-arc flux coordinate system.

Figure 11 compares the solutions at the end of the simulations shown in Fig. 10(a) and (d), in terms of the radial plasma displacement. The radial profiles of these poloidal harmonics show the mode structure. The unstable case, Fig. 11(b) with $q_a = 3.94$, shows an edge localised peeling mode structure. The stable case, Fig. 11(a) with $q_a = 4.33$, also has the peeling structure near the edge but in addition has a more global response in the plasma core.

We have performed quasi-linear simulations for all four cases, with both $n = 3$ and $n = 4$ RMP configurations. For each case, we also assume two different NTV models (the MARS-Q versus the MARS-K models). With the MARS-K model, we adopt a "perturbative" approach, where the fluid MHD equations are still solved for the plasma response, but only the NTV torque is computed via the MARS-K drift kinetic module. The eventual quasi-linear solution depends on the linear stability of the peeling mode. Generally, for cases where the peeling mode is linearly stable, we found little rotational damping due to the RMP fields, for both $n = 3$ and $n = 4$ configurations. For cases where the peeling mode is linearly unstable, the toroidal flow is locally damped near the plasma edge.

Figures 12 and 13 show one example of the stable peeling case, with the $n = 3$ configuration. The change of the rotation frequency, $\Delta\Omega$ shown in Fig. 12(a), is very small during the nonlinear evolution. The total rotation ($\Delta\Omega$ plus the initial equilibrium rotation frequency) almost does not change as shown in Fig. 12(b), for the rotation amplitude at all rational surfaces.

The solution fully saturates during the time period of $\sim$ 100ms, as shown in Fig. 13. The penetrated resonant field components saturate at a very small amplitude, of several Gauss level, indicating a good screening of the applied RMP field by the plasma flow in this case. The resulting net torques are also small. In particular, note that the saturated net NTV torque is about one order of magnitude smaller than the resonant electromagnetic ($\mathbf{j} \times \mathbf{b}$) torque. In this simulation, the MARS-Q model is used for computing the NTV torque. By switching to the MARS-K model, the resulting NTV torque is somewhat larger as shown in Fig. 14(b), but the final quasi-linear solution, in terms of the field penetration (Fig. 14(a)), as well as the rotation braking, remains almost the same. Full saturation of the quasi-linear solution, with almost no rotation braking, is also observed for the $n = 4$ RMP configuration.

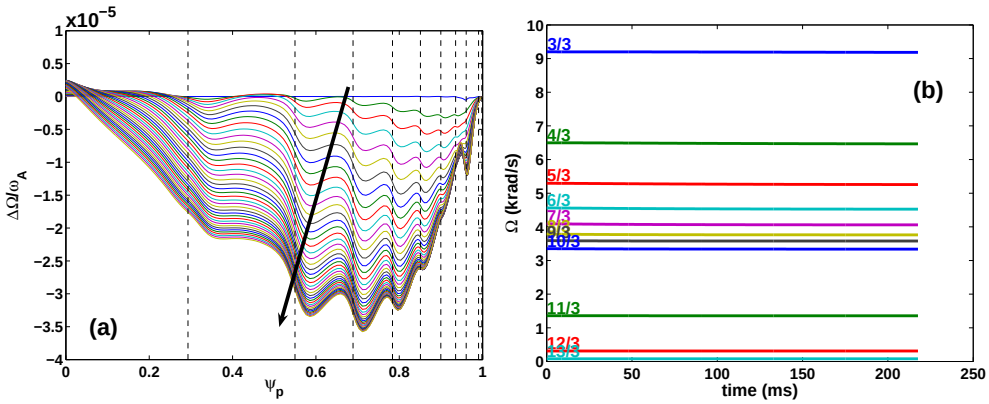

Figure 12: The evolution of the (a) rotation radial profile, and (b) rotation amplitude at rational surfaces, computed from the quasi-linear $n = 3$ RMP response simulations for the ITER equilibrium with q_a=4.33. The arrow in (a) indicates increasing time, for the time interval shown in (b). Note the very small magnitude of the change of the rotation frequency. The NTV torque is computed using the MARS-Q model based on analytic formulas.

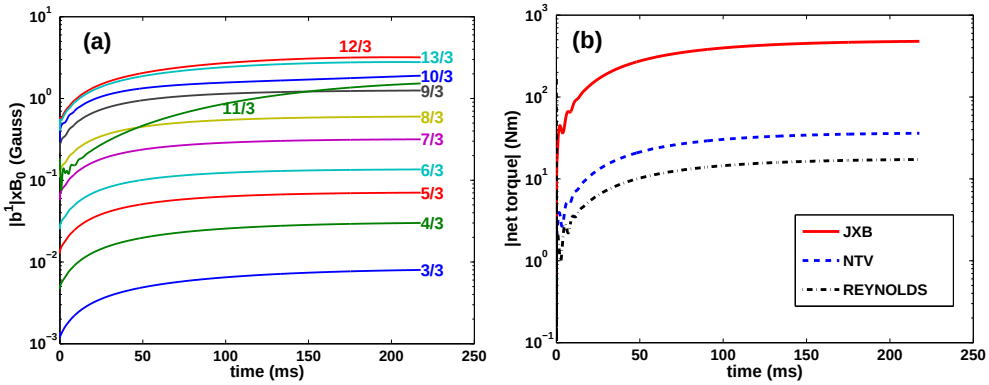

Figure 13: The evolution of the (a) amplitude of the resonant poloidal harmonics (in the PEST-like straight field line coordinate system) of the perturbed radial magnetic field, and (b) amplitude of the net torques acting on the plasma, computed from the quasi-linear $n = 3$ RMP response simulations for the ITER equilibrium with q_a=4.33. The NTV torque is computed using the MARS-Q model based on analytic formulas.

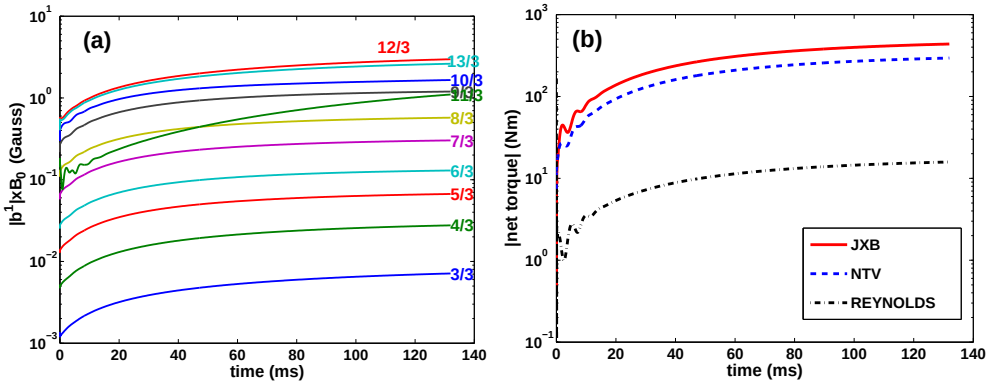

Figure 14: The evolution of the (a) amplitude of the resonant poloidal harmonics (in the PEST-like straight field line coordinate system) of the perturbed radial magnetic field, and (b) amplitude of the net torques acting on the plasma, computed from the quasi-linear $n = 3$ RMP response simulations for the ITER equilibrium with q_a=4.33. The NTV torque is computed using the full toroidal geometry based MARS-K model.

For both coil configurations, we also performed a sensitivity study by doubling the coil current. In these cases, still no appreciable rotation damping is obtained.

The quasi-linear solution is different with lower q_a values. Figures 15 and 16 show the solution at $q_a = 4.07$, where the peeling mode is linearly marginally unstable, as shown in Fig. 10(c). The quasi-linear run (Fig. 15) shows local damping of the toroidal flow near the plasma edge for this case. At about 35ms after the application of the $n = 3$ RMP field, the rotation amplitude in the region between the $q = 9/3$ rational surface and the plasma edge nearly vanishes. This is accompanied by the dynamic penetration of the resonant field components as shown in Fig. 16(a). Note that the amplitude of the resonant harmonics are shown here at each of the correspondent rational surfaces. The high poloidal number harmonics $m/n = 12/3, 11/3, 10/3$ have the largest amplitude. The simulation is terminated after the edge rotation is fully damped and the magnetic islands become large. This later stage cannot be properly captured by the quasi-linear model anymore. Similar rotation braking, but occurring at earlier time, is observed in the $q_a = 3.94$ case.

We point out that, even though only a local rotation damping is predicted in this simulation, his local rotation braking can nevertheless be important since it occurs in the edge pedestal region, where probably most interesting physics occur associated with the ELM mitigation by the RMP fields.

For the $n = 4$ configuration, the initial value runs show that the peeling mode is linearly stable for all the four cases considered in this work. At 30kAt nominal $n = 4$ RMP coil current, the quasi-linear response saturates as a low level of the field perturbation inside the plasma. The resulting weak torques do not lead to a noticeable damping of the plasma flow. In fact only with a much higher coil current, any edge braking of the flow is achieved. Figures 17 and 18 show one such an example, where we have assumed a 90kAt coil currents in the $n = 4$ configuration. A weak sound wave damping model is used. The MARS-K model is used for computing the NTV torque. The rotation damping is weaker and even more localised near the plasma edge, compared to that caused by the 45kAt $n = 3$ RMP fields.

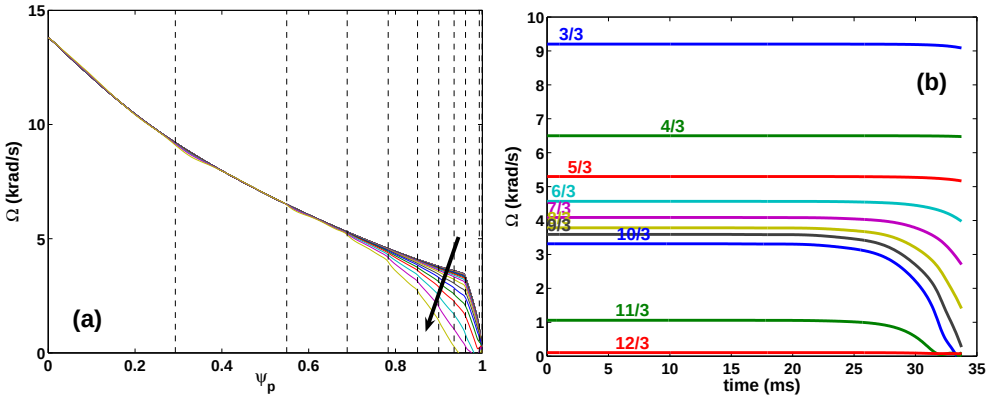

Figure 15: The evolution of the (a) rotation radial profile, and (b) rotation amplitude at rational surfaces, computed from the quasi-linear $n = 3$ RMP response simulations for the ITER equilibrium with q_a=4.07. The arrow in (a) indicates increasing time, for the time interval shown in (b). The NTV torque is computed using the MARS-Q model based on analytic formulas.

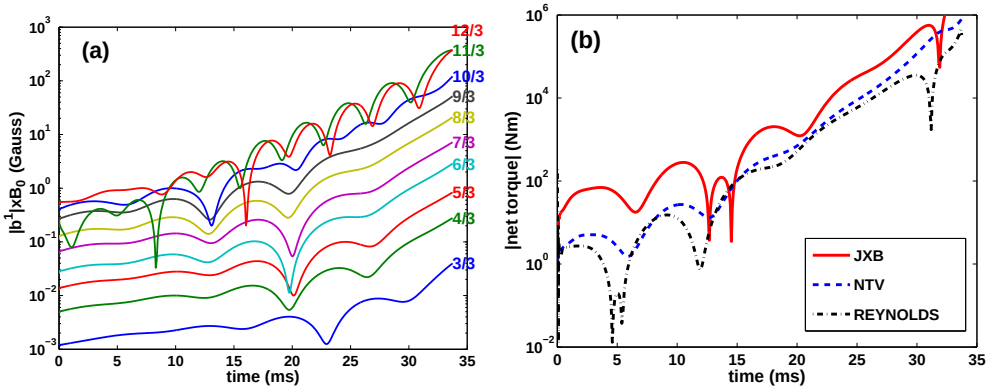

Figure 16: The evolution of the (a) amplitude of the resonant poloidal harmonics (in the PEST-like straight field line coordinate system) of the perturbed radial magnetic field, and (b) amplitude of the net torques acting on the plasma, computed from the quasi-linear $n = 3$ RMP response simulations for the ITER equilibrium with q_a=4.07. The NTV torque is computed using the MARS-Q model based on analytic formulas.

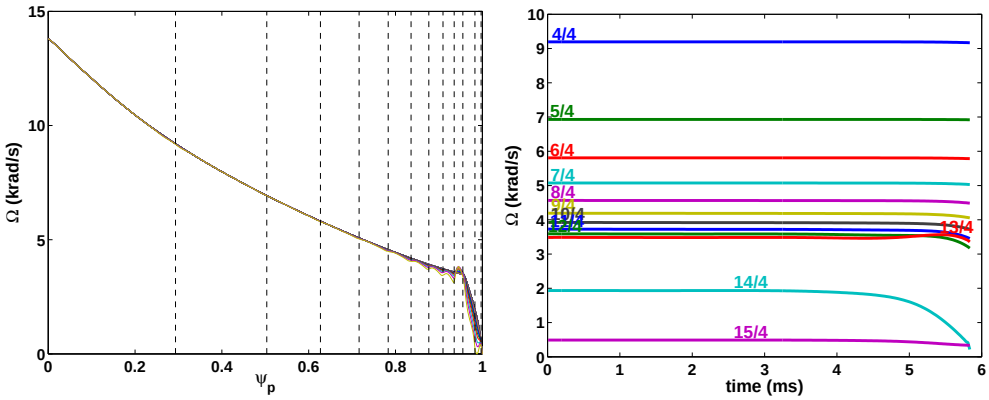

Figure 17: The evolution of the (a) rotation radial profile, and (b) rotation amplitude at rational surfaces, computed from the quasi-linear $n = 4$ RMP response simulations for the ITER equilibrium with q_a=3.94. The arrow in (a) indicates increasing time, for the time interval shown in (b). The NTV torque is computed using the MARS-Q model based on analytic formulas.

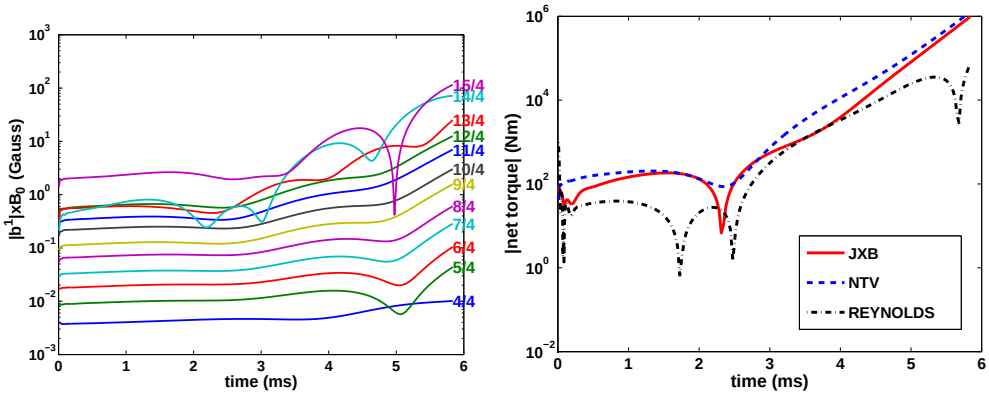

Figure 18: The evolution of the (a) amplitude of the resonant poloidal harmonics (in the PEST-like straight field line coordinate system) of the perturbed radial magnetic field, and (b) amplitude of the net torques acting on the plasma, computed from the quasi-linear $n = 4$ RMP response simulations for the ITER equilibrium with q_a=3.94. The NTV torque is computed using the MARS-Q model based on analytic formulas.

6 Summary and discussion

We have investigated both linear and quasi-linear response of an ITER plasma from the 15MA baseline scenario to the applied $n = 3$ and $n = 4$ RMP fields, using the MARS-F and the MARS-Q codes, respectively. The physics models that we assume are the single fluid model and the MHD-kinetic hybrid model. We solve full resistive MHD (as opposed to reduced MHD) equations with toroidal flow. The drift kinetic model and the pure fluid model produce similar response results, in terms of the total field perturbation inside the plasma as well as the plasma surface displacement for this ITER plasma, probably due to the fact that the plasma pressure for this baseline scenario is relatively low (well below the Troyon no-wall beta limits). Also, with the given RMP field configuration, our linear response computations do not show a strong kink response for the ITER plasma, contrary to the computational results obtained on some of the present day tokamaks [35, 20].

The drift kinetic model is also used to compute the NTV torque, which is compared to an analytic solution based model [25]. The results are similar. More importantly, both models show that the NTV torque is smaller than the resonant electromagnetic torque in this ITER plasma. In fact the latter provides a dominant momentum sink term for the flow damping in the quasi-linear simulations. The relatively weak NTV torque is related to the fact that the precessional drift resonance induced torque enhancement is largely absent. Therefore the non-resonant torque, which is often small, is mainly produced on the plasma.

The quasi-linear modelling with MARS-Q shows that, with 45kAt $n = 3$ RMP coil current, the toroidal flow can be damped, but only locally near the plasma edge. Furthermore, this local flow damping is sensitive to the existence of an initially weakly unstable edge localised peeling mode. We have carried out this sensitivity study by slightly varying the edge safety factor q_a across the integer number of 4, while keeping the bulk q-profile unchanged (in particular q_{95} is fixed at 3.18 as in the ITER target equilibrium). At q_a below 4, the $n = 3$ peeling mode is weakly unstable. This eventually causes the rotation braking near the plasma edge in the quasi-linear simulations. As q_a exceeds about 4.1, the $n = 3$ peeling modes are linearly stable. The quasi-linear runs show full saturation of the solution with very little rotation braking. In the ideal case, the presence of an exact X-point in the divertor configuration leads to a marginally stable peeling mode. The resulting rotational damping, if any, is probably weaker than that predicted for the case with a weakly unstable peeling mode. The $n = 4$ peeling mode seems to be stable for all four q_a values considered in this work, thus leading to the full saturation of the quasi-linear solution. With 30kAt $n = 4$ coil current, little flow damping is predicted for this ITER plasma.

In this study, we have not yet included the influence of the low-n error field in ITER on the plasma response. In the quasi-linear model, we neglected the torque due to energetic particles and the torque associated with the intrinsic flow. The intrinsic momentum flux has been shown to have an interesting effect on the radial profile of the plasma toroidal rotation profile, e.g. by inducing rotation reversal due to the collision regime change (from banana to the plateau regime) in Ohmic plasmas [42]. The role of this intrinsic momentum flux in the ITER H-mode plasma, that we studied here, is not clear. At any rate, the rotation reversal may not occur in ITER, since the ion collision frequency is rather low (we have estimated that the ν_* value is below 0.1 for $s \equiv \sqrt{\psi_p} \in [0.04, 0.99]$ for this ITER equilibrium). It is, on the other hand, interesting to understand how the presence of the 3D RMP field can change the intrinsic

momentum flux. Such a model is not available yet.

Acknowledgements

This project has received funding from the European Union's Horizon 2020 research and innovation programme under grant agreement number 633053 and from the RCUK Energy Programme [grant number EP/I501045]. Work is also part funded by National Natural Science Foundation of China (NSFC) [grant number 11428512]. The views and opinions expressed herein do not necessarily reflect those of the European Commission or the ITER Organization.

References

[1] Fitzpatrick R. 1993 *Nucl. Fusion* **33** 1049

[2] Evans T.E. *et al* 2006 *Nat. Phys.* **2** 419

[3] Loarte A. *et al* 2007 *Nucl. Fusion* **47** S203

[4] Liang Y. *et al* 2007 *Phys. Rev. Lett.* **98** 265004

[5] Nardon E. *et al* 2009 *Plasma Phys. Control. Fusion* **51** 124010

[6] Kirk A. *et al* 2010 *Nucl. Fusion* **50** 034008

[7] Suttrop W. *et al* 2011 *Phys. Rev. Lett.* **106** 225004

[8] Schaffer M. *et al* 2008 *Nucl. Fusion* **48** 024004

[9] Liu Y.Q. *et al* 2010 *Phys. Plasmas* **17** 122502

[10] Ferraro N.M. 2012 *Phys. Plasmas* **19** 056105

[11] Waelbroeck F.L. *et al* 2012 *Nucl. Fusion* **52** 074004

[12] Liu Y.Q. *et al* 2008 *Phys. Plasmas* **15** 112503

[13] Park G. *et al* 2010 *Phys. Plasmas* **17** 102503

[14] Huysmans G. *et al* 2007 *Nucl. Fusion* **47** 659

[15] Becoulet M. *et al* 2012 *Nucl. Fusion* **52** 054003

[16] Orain F. *et al* 2013 *Phys. Plasmas* **20** 102510

[17] Park J.-K. *et al* 2007 *Phys. Rev. Lett.* **99** 195003

[18] Turnbull A. *et al* 2013 *Phys. Plasmas* **20** 056114

[19] Heyn M.F. *et al* 2008 *Nucl. Fusion* **48** 024005

[20] Haskey S. *et al* 2014 *Plasma Phys. Control. Fusion* **56** 035005

[21] Chapman I.T. *et al* 2007 *Nucl. Fusion* **47** L36

[22] Liu Y.Q. *et al* 2011 *Nucl. Fusion* **51** 083002

[23] Chapman I.T. *et al* 2012 *Plasma Phys. Control. Fusion* **54** 105013

[24] Liu Y.Q. *et al* 2013 *Phys. Plasmas* **20** 042503

[25] Shaing K.C. *et al* 2010 *Nucl. Fusion* **50** 025022

[26] Sun Y. *et al* 2010 *Phys. Rev. Lett.* **105** 145002

[27] Hirshman S.P. *et al* 1983 *Phys. Fluids* **26** 3553

[28] ITER private communications, ABT4ZL, version 1.0

[29] Suzuki Y. *et al* 2006 *Nucl. Fusion* **46** L19

[30] Lanctot M. *et al* 2010 *Phys. Plasmas* **17** 030701

[31] Wang Z.R. *et al* 2014 *Phys. Rev. Lett.* submitted

[32] Berkery J.W. *et al* 2014 *Phys. Plasmas* **21** 056105

[33] Park J.-K. 2011 *Phys. Plasmas* **18** 110702

[34] Wang Z.R. *et al* 2014 *Phys. Plasmas* **21** 042502

[35] Liu Y.Q. *et al* 2012 *Plasma Phys. Control. Fusion* **54** 124013

[36] Crotinger J. *et al* "Corsica: A comprehensive simulation of toroidal magnetic fusion devices. Final report to the LDRD program" 1997 *Tech. Rep. (Lawrence Livermore National Lab. CA (United States)*

[37] Evans T.E. *et al* 2013 *Nucl. Fusion* **53** 093029

[38] Liu Y.Q. *et al* 2010 *Plasma Phys. Control. Fusion* **52** 045011

[39] Huysmans G.T.A. *et al* 2005 *Plasma Phys. Control. Fusion* **47** 2107

[40] Webster A.J. *et al* 2009 *Phys. Rev. Lett.* **102** 035003

[41] R.V. Budny *et al* 2008 *Nucl. Fusion* **48** 075005

[42] Barnes M. *et al* 2013 *Phys. Rev. Lett.* **111** 055005